

Crystal structure of the 3C protease from South African Territories type 2 foot-and-mouth disease virus

Jingjie Yang, Eoin N Leen, Francois F Maree, Stephen Curry

The replication of foot-and-mouth disease virus (FMDV) is dependent on the virus-encoded 3C protease ($3C^{pro}$). As in other picornaviruses, $3C^{pro}$ performs most of the proteolytic processing of the polyprotein expressed from the single open reading frame in the RNA genome of the virus. Previous work revealed that the $3C^{pro}$ from serotype A -one of the seven serotypes of FMDV - adopts a trypsin-like fold. Phylogenetically the FMDV serotypes are grouped into two clusters, with O, A, C, and Asia 1 in one, and the three South African Territories serotypes, (SAT-1, SAT-2 and SAT-3) in another. We report here the cloning, expression and purification of 3C proteases from four SAT serotype viruses (SAT2/GHA/8/91, SAT1/NIG/5/81, SAT1/UGA/1/97, and SAT2/ZIM/7/83) and the crystal structure at 3.2Å resolution of $3C^{pro}$ from SAT2/GHA/8/91).

1 **Crystal structure of the 3C protease from South African**
2 **Territories type 2 foot-and-mouth disease virus**

3

4 **Jingjie Yang¹, Eoin N. Leen^{1#}, François F. Maree² and Stephen Curry^{1*}**

5

6 ¹Department of Life Sciences, Sir Ernst Chain Building, Imperial College, Exhibition Road,
7 London SW7 2AZ, United Kingdom.

8 ²Transboundary Animal Disease Programme, Agricultural Research Council, Onderstepoort
9 Veterinary Institute, Private Bag X05, Onderstepoort, 0110, South Africa.

10 ³Department of Microbiology and Plant Pathology, Faculty of Agricultural and Natural
11 Sciences, University of Pretoria, Pretoria, 0002, South Africa.

12 #Present address: Astbury Building, University of Leeds, Woodhouse, Leeds LS2 9LU, UK

13

14 *Corresponding author: s.curry@imperial.ac.uk

15

16 Keywords: foot-and-mouth disease virus, 3C protease, crystal structure, structural
17 conservation, drug target.

19 **ABSTRACT**

20 The replication of foot-and-mouth disease virus (FMDV) is dependent on the virus-encoded
21 3C protease (3C^{pro}). As in other picornaviruses, 3C^{pro} performs most of the proteolytic
22 processing of the polyprotein expressed from the single open reading frame in the RNA
23 genome of the virus. Previous work revealed that the 3C^{pro} from serotype A – one of the
24 seven serotypes of FMDV – adopts a trypsin-like fold. Phylogenetically the FMDV serotypes
25 are grouped into two clusters, with O, A, C, and Asia 1 in one, and the three South African
26 Territories serotypes, (SAT-1, SAT-2 and SAT-3) in another. We report here the cloning,
27 expression and purification of 3C proteases from four SAT serotype viruses
28 (SAT2/GHA/8/91, SAT1/NIG/5/81, SAT1/UGA/1/97, and SAT2/ZIM/7/83) and the
29 crystal structure at 3.2 Å resolution of 3C^{pro} from SAT2/GHA/8/91).

30

31

32 INTRODUCTION

33 Diseases caused by RNA viruses are often difficult to control because of the high mutation
34 rate and the continual emergence of novel genetic and antigenic variants that escape from
35 immune surveillance. The degree to which immunity induced by one virus is effective
36 against another is largely dependent on the antigenic differences between them. Foot-and-
37 mouth disease virus (FMDV) is an example of an antigenically variable pathogen that
38 infects many species of cloven-hoofed animals, such as cattle, sheep, pigs and goats, and
39 remains a potent threat to agricultural livestock (Sutmoller et al., 2003). Although FMD
40 vaccines made from chemically inactivated virus particles are in widespread use, control of
41 the disease remains difficult. This is because the vaccines provide only short-lived
42 protection and the virus occurs as seven clinically indistinguishable serotypes (O, A, C,
43 Asia1 and three South African Territories serotypes: SAT1, SAT2 and SAT3), each of which
44 has multiple, constantly evolving sub-types (Knowles & Samuel, 2003). Viruses belonging
45 to the SAT serotypes display appreciably greater genomic and antigenic variation compare
46 to serotype A and O viruses (Bastos et al., 2001; Bastos et al., 2003; Maree et al. 2011),
47 possibly due to their long term maintenance within African buffalo (*Syncerus caffer*).
48 Constant surveillance of circulating strains is required to ensure that vaccine stocks remain
49 effective.

50 In common with other members of the picornavirus family, FMDV has a single-stranded,
51 positive-sense RNA genome with just one open reading frame. Cell entry in infected hosts is
52 followed immediately by translation of the viral RNA, which yields a polyprotein precursor
53 of over 2,000 amino acids that has to be processed into fourteen distinct capsid and non-

54 structural proteins for virus replication. The majority of this processing is done by the
55 virus-encoded 3C protease (3C^{pro}), which cleaves the precursor at ten distinct sites
56 (reviewed in Curry et al., 2007).

57 Crystallographic analysis of the 3C^{pro} from a type A FMDV (sub-type A10₆₁) showed that,
58 similar to other picornavirus 3C proteases, it adopts a trypsin-like fold consisting of two β-
59 barrels that pack together to create a centrally-located Cys-His-Asp/Glu catalytic triad in
60 the active site (Allaire et al., 1994; Matthews et al., 1994; Mosimann et al., 1997; Birtley et
61 al., 2005; Yin et al., 2005). Subsequent studies on FMDV 3C^{pro} complexed with peptides
62 derived from the viral polyprotein work revealed that substrate recognition is achieved by
63 conformational changes primarily involving the movement of a β-ribbon (residues 138-
64 150) that helps to secure the position of cognate peptides in relation to the active site of the
65 protein (Sweeney et al., 2007; Zunszain et al., 2010).

66 Mapping of the sequence variation between different FMDV serotypes onto the structure of
67 A10₆₁ 3C^{pro} indicated that the peptide-binding face of the protease is completely conserved
68 among the non-SAT serotypes (which are 91-97% conserved in amino-acid sequence),
69 supporting the notion that identification of inhibitors of the protease might aid the
70 development of broad spectrum antiviral drugs (Birtley et al., 2005; Curry et al., 2007).

71 This structure should therefore serve as a useful model for the 3C protease from this group
72 of viruses. However, the same comparison suggested the presence of at least two amino
73 acid differences on the peptide-binding surfaces between A10₆₁ 3C^{pro} and the
74 corresponding 3C sequences from SAT serotype viruses.

75 To provide a more complete picture of the structural variation between FMDV 3C proteases
76 from different serotypes, we set out to determine the crystal structure of 3C^{pro} from at least
77 one SAT serotype virus. We report here the cloning and expression of 3C^{pro} from four
78 distinct SAT1 and SAT2 viruses and the crystal structure of the 3C^{pro} from a SAT2 serotype
79 virus (SAT2/GHA/8/91).

80

81 **MATERIALS AND METHODS**

82 **Cloning and mutagenesis:** We used the polymerase chain reaction (PCR) to amplify the
83 coding regions for the FMDV 3C proteases of sub-types SAT2/GHA/8/91 (Accession No.
84 AY884136), SAT1/NIG/5/81 (Accession No. AY882592), SAT1/UGA/1/97 (Accession No.
85 AF283456), and SAT2/ZIM/7/83 (Accession No. AF540910). In each case the reaction was
86 performed using DNA primers (Table 1) that introduced 5' *Xho*I and a 3' *Hind*III restriction
87 sites into the PCR products. These served to facilitate ligation into a version of the pETM-11
88 vector that had been modified to insert a thrombin cleavage site immediately downstream
89 of the N-terminal His tag (Birtley & Curry, 2005). DNA ligations were performed using the
90 Roche Rapid Ligation Kit according to the manufacturer's instructions.

91 Site-directed mutagenesis was performed with the Quikchange method (Stratagene), using
92 KOD polymerase (Novagen). All DNA sequences were verified by sequencing.

93 **Protein Expression and Purification:** All SAT-type 3C proteases were expressed in
94 cultures of BL21 (DE3) pLysS *E. coli* (Invitrogen) grown in lysogeny broth (LB) at 37°C with
95 shaking at 225 rpm. Protein expression was induced for 5 hours by the addition of 1 mM

96 isopropyl β -d-1-thiogalactopyranoside (IPTG) once the optical density at 600 nm reached
97 0.8-1.0. Cells were harvested by centrifugation at 4550 g for 15 min at 4°C and frozen at –
98 80 °C.

99 The volumes given below are appropriate for processing the pellet from 1 L of bacterial
100 culture. Cell pellets were thawed on ice and re-suspended in 30 mL Buffer A (50 mM HEPES
101 pH7.1, 400 mM NaCl, 1 mM β -mercaptoethanol) supplemented with 0.1% Triton X-100 and
102 1 mM phenylmethylsulfonyl fluoride (PMSF) protease inhibitor. Cells were lysed by
103 sonication on ice and lysates clarified by centrifugation at 29,000 g for 20 min at 4°C.
104 Protamine Sulphate (Sigma) was added to 1 mg/ml final concentration to precipitate
105 nucleic acids, and lysates were then centrifuged again at 29,000 g for 20 min. The
106 supernatant was filtered using a 1.2 μ m syringe filter and incubated for 90 minutes at 4°C
107 with slow rotation in 1 mL bed volume of TALON metal affinity resin (Clontech) pre-
108 equilibrated with buffer A. This slurry was applied to a gravity-flow column and the TALON
109 beads washed three times with 50 mL of Buffer A supplemented with 0, 5 and 10 mM
110 imidazole respectively. His-tagged 3C proteins were eluted in 20 ml of Buffer A containing
111 100 mM imidazole, followed by a final wash with 10 ml of Buffer A containing 250 mM
112 imidazole. To remove the His tag the eluted protein was mixed with 100 units of bovine
113 thrombin (Sigma) and dialysed for 16 hr at 4°C in 4 L of Buffer A supplemented with 2 mM
114 CaCl_2 . Cleaved protein was then re-applied to TALON resin to remove the cleaved His tag
115 and other contaminants. The untagged protease was recovered in the flow through,
116 concentrated using Vivaspin concentrators (3 kD MWCO) (Sartorius Stedim Biotech) and
117 further purified by gel filtration using HiLoad 16/60 Superdex 75 gel filtration column
118 (Amersham Bioscience) in Buffer A supplemented with 1 mM EDTA and 0.01% sodium

119 azide at flow rate of 0.5 ml/min. Peak fractions were pooled, concentrated and stored at –
120 80 °C. Protein concentrations were determined from absorbance measurements at 280 nm
121 using extinction coefficients calculated with the ProtParam tool (Gastiger et al., 2005).

122 **Crystallisation and structure determination:** Crystallisation trials with purified SAT-
123 type 3C^{pro} were performed at 4°C and 18°C using protein concentrations in the range 5-
124 10 mg/mL. Initial screens were done by sitting drop vapour diffusion using a Mosquito
125 crystallisation robot (TTP Labtech). Typically in each drop 100 nl of protein was mixed
126 with 100nl taken from the 100 µL reservoir solution. Trials were performed with the
127 following commercial screens: Crystal screen 1 and 2, and PEG/Ion (Hampton Research);
128 Memstart, Memcys, JCSG+, and PACT (Molecular Dimensions); Wizard 1 and 2 (Rigaku
129 Reagents).

130 Crystals of g3C-SAT2-G(1-208) for data collection were washed in the mother liquor (15%
131 (w/v) PEG-8000, 0.09 M Na-cacodylate pH 7.0, 0.27 M Ca-acetate, 0.01 M Tris pH 8.5, 0.08
132 M Na-thiocyanate) supplemented with 20% (v/v) glycerol, and immediately frozen in
133 liquid nitrogen in a nylon loop. X-ray diffraction data were processed and scaled with the
134 CCP4 program suite (Collaborative Computer Project No. 4, 1994), and phased by
135 molecular replacement using the coordinates of type A10₆₁ FMDV 3C^{pro} (PDB ID 2j92;
136 (Sweeney et al., 2007)) as a search model in Phaser (McCoy et al., 2007). The search model
137 was edited to delete side-chains (to the C_β atom) for all residues that differed with g3C-
138 SAT2-G(1-208) and to remove all the atoms in the β-ribbon (residues 138-150), since these
139 have been observed to vary in structure between different crystal forms (Sweeney et al.,
140 2007). Model building and adjustments were done using Coot (Emsley et al., 2010);

141 crystallographic refinement was performed initially with CNS (Brünger et al., 1998) and
142 completed using Phenix (Adams et al., 2010).

143

144 **RESULTS AND DISCUSSION**

145 **Protein expression and crystallisation:** We engineered bacterial expression plasmids for
146 FMDV 3C proteases from four SAT sub-types: SAT2/GHA/8/91, SAT1/NIG/5/81,
147 SAT1/UGA/1/97, and SAT2/ZIM/7/83 (see Materials and Methods). In doing so we were
148 guided by the lessons learned from work to express and crystallise subtype A10₆₁ FMDV
149 3C^{pro}, which suggested that preserving the N terminus of the protein but truncating the C
150 terminus by up to six residues would be optimal for solubility and crystallisation (Birtley &
151 Curry, 2005). Accordingly, for each SAT sub-type we generated expression constructs that
152 add a thrombin-cleavable His tag to the N terminus of residues 1-208 of the 213 amino acid
153 3C protease; following thrombin cleavage there is a single additional Gly residue appended
154 to the N terminus of the protease polypeptide. To ensure the solubility of the SAT-type 3C
155 proteins, we introduced to all constructs a C142A substitution to remove a surface-exposed
156 Cys that had been shown previously to be responsible for protein aggregation (Birtley &
157 Curry, 2005; Birtley et al., 2005). (The C95K mutation also introduced to eliminate
158 aggregation of A10₆₁ FMDV 3C^{pro} (Birtley & Curry, 2005) was not needed here because
159 residue 95 is an Arg in the SAT 3C proteases used in this study). In addition, the active site
160 nucleophile was eliminated from all constructs by incorporation of a C163A substitution to
161 prevent adventitious proteolysis in highly concentrated samples of purified 3C^{pro}. For
162 consistency with our earlier naming scheme these SAT2/GHA/8/91, SAT1/NIG/5/81,

163 SAT1/UGA/1/97, and SAT2/ZIM/7/83 3C constructs will be referred to as SAT2/G-
164 g3C^{pro}(1-208), SAT1/N-g3C^{pro}(1-208), SAT1/U- g3C^{pro}(1-208), and SAT2/Z- g3C^{pro}(1-208)
165 respectively.

166 The 3C^{pro} proteins from all four SAT sub-types yielded soluble protein that was purified
167 first by metal-affinity chromatography and then following thrombin cleavage of the
168 N-terminal His tag, on a gel filtration column (see Materials and Methods). Of the four,
169 SAT1/N-g3C^{pro}(1-208) appeared to be the most soluble and could be concentrated to
170 20 mg/mL. The other three variants exhibited some precipitation during gel filtration,
171 indicated by a void peak containing aggregated 3C^{pro}, which was about one-third of the area
172 of the monomeric peak. They also had lower apparent solubility limits and could be
173 concentrated to ~6 mg/mL [SAT2/G-g3C^{pro}(1-208)] or ~11 mg/mL [SAT1/U- g3C^{pro}(1-
174 208), and SAT2/Z- g3C^{pro}(1-208)].

175 In crystallisation trials we only obtained crystals from the 3C^{pro} of a single sub-type:
176 SAT2/G-g3C^{pro}(1-208). These exhibited a variety of habits but the largest were needle-
177 shaped and were typically 10 µm wide and up to 300 µm long. In initial diffraction tests on
178 beamline ID23-2 at the European Synchrotron Radiation Facility (ESRF) showed that the
179 crystals belonged to a trigonal spacegroup and diffracted to a resolution limit of 2 Å.
180 Unfortunately, for reasons that remain unclear, efforts to reproduce these crystals proved
181 troublesome. In subsequent trials diffraction was limited to ~3 Å.

182 We used mutagenesis to engineer modifications to the SAT2/G-g3C^{pro}(1-208) construct in
183 the search for better crystals. Although alterations to trim the C-terminus by one residue
184 [in SAT2/G-g3C^{pro}(1-207)], or to add back a single His residue [in SAT2/G-g3C^{pro}(1-207h)]

185 – strategies that had been useful when working with type A10₆₁ 3C^{pro} (Birtley & Curry,
186 2005) — both yielded soluble protein and SAT2/G-g3C^{pro}(1-207h) produced crystals, there
187 was no improvement in the resolution of the diffraction.

188 In a further effort to enhance crystal quality, we used the Surface Entropy Reduction
189 prediction server (Goldschmidt et al., 2007) to design additional SAT2/G-g3C^{pro}(1-208)
190 mutants. We made four different mutants, each containing the following pairs of
191 substitutions: (i) K110T/K111Y (ii) K110Y/K111T; (iii) K51A/K54Y; (iv) K51T/K54S. Of
192 these, only the K51A/K54Y mutant gave protein that was as soluble as wild-type. The
193 K110T/K111Y and K51T/K54S double-mutants produced significantly larger void peaks
194 during purification by gel filtration chromatography, while the K110Y/K111T double-
195 mutant appeared almost entirely aggregated under these conditions. For the three surface-
196 entropy mutants that did yield soluble protein, no useable crystals were obtained.

197 **Structure of SAT2/G-g3C^{pro}(1-208):** A complete dataset to 3.2 Å resolution was obtained
198 from crystals of SAT2/G-g3C^{pro}(1-208). The crystals belong to space-group P3₂ and have a
199 long c-axis (318.5 Å). The diffraction data were phased by molecular replacement using a
200 search model based on the crystal structure of type A10₆₁ FMDV 3C^{pro}, which is 80%
201 identical in amino-acid sequence to SAT2/G-g3C^{pro}(1-208) (see Materials and Methods).
202 This gave an unambiguous solution with a log likelihood gain of 1495 (McCoy et al., 2007),
203 revealing five molecules in the asymmetric unit. Though of modest resolution, the initial
204 electron density maps were of sufficient quality to guide adjustment of the initial molecular
205 replacement model prior to multiple interleaved rounds of refinement and model building
206 (Fig. 1a). Because of the limited resolution and non-crystallographic symmetry, refinement

207 was performed using group B-factors and non-crystallographic restraints. Model building
208 was done conservatively – amino acid side-chains were truncated to the C_β atom in cases
209 where there was no indicative electron density. The final model of SAT2/G-g3C^{pro}(1-208)
210 contains residues 7-207 for all five chains and has an R_{free} of 27.2% and good
211 stereochemistry; full data collection and refinement statistics are given in Table 1.

212 As expected, given the high level of amino acid sequence identity with A10₆₁ 3C^{pro}, FMDV
213 SAT2/G-g3C^{pro}(1-208) adopts the same trypsin-like fold (Fig. 1b), which has been
214 described in detail elsewhere (Birtley et al., 2005; Sweeney et al., 2007). Superposition of
215 the five molecules in the asymmetric unit shows that they are highly similar to one another
216 (Fig. 1c) – the pair-wise root mean square deviation in C_α positions between chains is 0.2-
217 0.3 Å. The largest differences are observed in the longest surface-exposed loops, the E₁-F₁
218 loop in the N-terminal β-barrel and the B₂-C₂ loop known as the β-ribbon in the C-terminal
219 β-barrel (Fig. 1c). These are also the regions of greatest difference between SAT2/G-
220 g3C^{pro}(1-208) and A10₆₁ 3C^{pro}; (overlay of the two structures yields an overall rms
221 deviation in C_α positions of ~0.6 Å) (Fig. 1d). The flexibility of the β-ribbon, which shifts in
222 position to aid peptide binding, has been noted before (Zunszain et al., 2010) and clearly it
223 plays a similar role in SAT-type 3C proteases.

224

225 **CONCLUDING REMARKS**

226 The results reported here provide a template structure of a SAT-type FMDV 3C protease
227 that should be of value in directing molecular investigations of this group of proteases.

228 Although it is frustrating that higher-resolution diffraction data were not obtained, given
229 that initial crystals of SAT2/G-g3C^{pro}(1-208) diffracted to 2 Å, this should be possible with
230 further optimization. Likewise, since soluble 3C^{pro} was found to be purified from three
231 other SAT-type viruses – notably SAT1/NIG/5/81 – crystal structures for these proteases
232 may well also be achievable. This work has applications in the use of reverse genetics
233 approaches or the design of empty virus capsids to target antigenically significant subtypes
234 in the design of regional vaccines for the control of FMD (Porta et al., 2013).

235

236 **ACKNOWLEDGEMENTS**

237 We thank staff on beamline ID23 at the ESRF for assistance with data collection. This work
238 was supported by the award of a Wellcome Trust studentship (to E.N.L.) (reference:
239 083248/2/07/2).

240

241

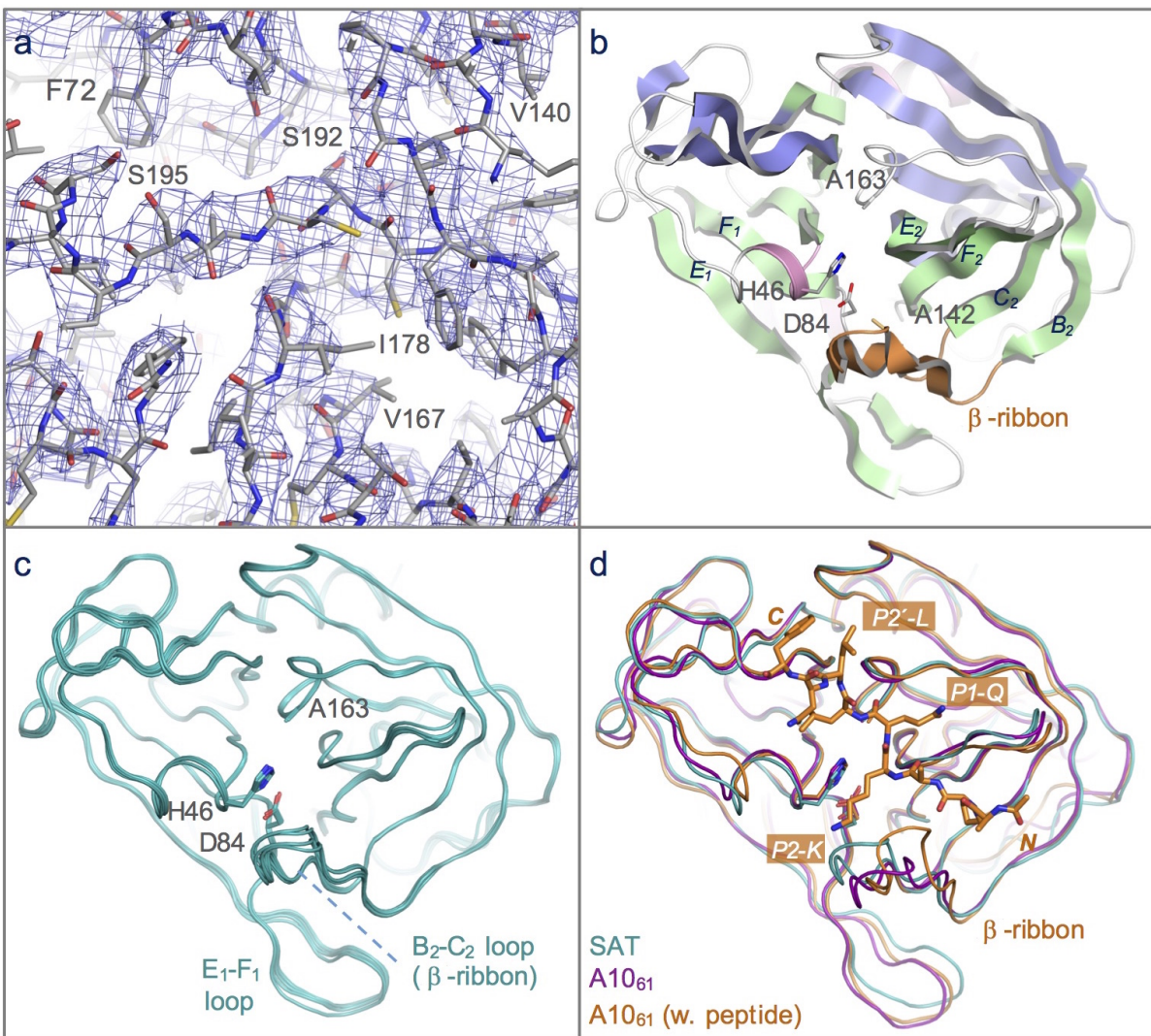
242

243 **REFERENCES**

- 244 Adams PD, Afonine PV, Bunkoczi G, Chen VB, Davis IW, Echols N, Headd JJ, Hung LW, Kapral GJ,
245 Grosse-Kunstleve RW, McCoy AJ, Moriarty NW, Oeffner R, Read RJ, Richardson DC, Richardson
246 JS, Terwilliger TC, and Zwart PH. 2010. PHENIX: a comprehensive Python-based system for
247 macromolecular structure solution. *Acta Crystallogr D Biol Crystallogr* 66:213-221.
- 248 Allaire M, Chernaia MM, Malcolm BA, and James MN. 1994. Picornaviral 3C cysteine proteinases
249 have a fold similar to chymotrypsin-like serine proteinases. *Nature* 369:72-76.
- 250 Bastos AD, Haydon DT, Forsberg R, Knowles NJ, Anderson EC, Bengis RG, Nel LH, and Thomson GR. 2001.
251 Genetic heterogeneity of SAT-1 type foot-and-mouth disease viruses in southern Africa. *Arch Virol*
252 146:1537-1551.
- 253 Bastos AD, Anderson EC, Bengis RG, Keet DF, Winterbach HK, and Thomson GR. 2003. Molecular
254 epidemiology of SAT3-type foot-and-mouth disease. *Virus Genes* 27:283-290.
- 255 Birtley JR, and Curry S. 2005. Crystallization of foot-and-mouth disease virus 3C protease: surface
256 mutagenesis and a novel crystal-optimization strategy. *Acta Crystallogr D Biol Crystallogr*
257 61:646-650.
- 258 Birtley JR, Knox SR, Jaulent AM, Brick P, Leatherbarrow RJ, and Curry S. 2005. Crystal structure of
259 foot-and-mouth disease virus 3C protease. New insights into catalytic mechanism and cleavage
260 specificity. *J Biol Chem* 280:11520-11527.
- 261 Brünger AT, Adams PD, Clore GM, DeLano WL, Gros P, Grosse-Kunstleve RW, Jiang JS, Kuszewski J,
262 Nilges M, Pannu NS, Read RJ, Rice LM, Simonson T, and Warren GL. 1998. Crystallography &
263 NMR system: A new software suite for macromolecular structure determination. *Acta*
264 *Crystallogr.* D54:905-921.
- 265 Collaborative Computer Project No. 4. 1994. The CCP4 suite: programs for protein crystallography.
266 *Acta Crystallogr. D* 50:760-763.
- 267 Curry S, Roque-Rosell N, Sweeney TR, Zunszain PA, and Leatherbarrow RJ. 2007. Structural analysis
268 of foot-and-mouth disease virus 3C protease: a viable target for antiviral drugs? *Biochem Soc*
269 *Trans* 35:594-598.
- 270 Emsley P, Lohkamp B, Scott WG, and Cowtan K. 2010. Features and development of Coot. *Acta*
271 *Crystallogr D Biol Crystallogr* 66:486-501.
- 272 Engh RA, and Huber R. 1991. Accurate bond and angle parameters for x-ray protein-structure
273 refinement. *Acta Crystallogr.* A47:392-400.
- 274 Gastiger E, Hoogland C, Gattiker A, Duvaud S, Wilkins MR, Appel RD, and Bairoch A. 2005. Protein
275 Identification and Analysis Tools on the ExPASy Server. In: Walker JM, ed. *The Proteomics*
276 *Protocols Handbook*. Totowa, NJ: Humana Press Inc., 571-607.

- 277 Goldschmidt L, Cooper DR, Derewenda ZS, and Eisenberg D. 2007. Toward rational protein
278 crystallization: A Web server for the design of crystallizable protein variants. *Protein Sci*
279 16:1569-1576.
- 280 Knowles NJ, and Samuel AR. 2003. Molecular epidemiology of foot-and-mouth disease virus. *Virus*
281 *Res* 91:65-80.
- 282 Matthews DA, Smith WW, Ferre RA, Condon B, Budahazi G, Sisson W, Villafranca JE, Janson CA,
283 McElroy HE, Gribskov CL, and Worland S. 1994. Structure of human rhinovirus 3C protease
284 reveals a trypsin-like polypeptide fold, RNA-binding site, and means for cleaving precursor
285 polyprotein. *Cell* 77:761-771.
- 286 McCoy AJ, Grosse-Kunstleve RW, Adams PD, Winn MD, Storoni LC, and Read RJ. 2007. Phaser
287 crystallographic software. *J Appl Crystallogr* 40:658-674.
- 288 Maree FF, Blignaut B, Esterhuysen JJ, de Beer TA, Theron J, O'Neill HG, and Rieder E. 2011. Predicting
289 antigenic sites on the foot-and-mouth disease virus capsid of the South African Territories types
290 using virus neutralization data. *J Gen Virol* 92:2297-2309.
- 291 Mosimann SC, Cherney MM, Sia S, Plotch S, and James MN. 1997. Refined X-ray crystallographic
292 structure of the poliovirus 3C gene product. *J Mol Biol* 273:1032-1047.
- 293 Porta C, Xu X, Loureiro S, Paramasivam S, Ren J, Al-Khalil T, Burman A, Jackson T, Belsham GJ, Curry S et al. .
294 2013. Efficient production of foot-and-mouth disease virus empty capsids in insect cells following
295 down regulation of 3C protease activity. *J Virol Methods* 187:406-412.
- 296 Suttmoller P, Barteling SS, Olascoaga RC, and Sumption KJ. 2003. Control and eradication of foot-
297 and-mouth disease. *Virus Res* 91:101-144.
- 298 Sweeney TR, Roque-Rosell N, Birtley JR, Leatherbarrow RJ, and Curry S. 2007. Structural and
299 mutagenic analysis of foot-and-mouth disease virus 3C protease reveals the role of the beta-
300 ribbon in proteolysis. *J Virol* 81:115-124.
- 301 Yin J, Bergmann EM, Cherney MM, Lall MS, Jain RP, Vederas JC, and James MN. 2005. Dual modes of
302 modification of hepatitis A virus 3C protease by a serine-derived beta-lactone: selective
303 crystallization and formation of a functional catalytic triad in the active site. *J Mol Biol* 354:854-
304 871.
- 305 Zunszain PA, Knox SR, Sweeney TR, Yang J, Roque-Rosell N, Belsham GJ, Leatherbarrow RJ, and
306 Curry S. 2010. Insights into cleavage specificity from the crystal structure of foot-and-mouth
307 disease virus 3C protease complexed with a peptide substrate. *J Mol Biol* 395:375-389.
308

309

310 **FIGURE**

311

312 **Figure 1: Structure of the 3C protease from the SAT2/GHA/8/91 serotype FMDV.**

313 (a) Section of the 3.2 Å resolution electron density map (blue chicken wire) calculated with
 314 phases from the final refined model, which is shown as sticks coloured by atom type: grey –
 315 carbon; red – oxygen; blue – nitrogen; yellow – sulphur. (b) Overall structure of SAT2/G-
 316 g3C^{pro}(1-208), with secondary structure elements indicated. (c) Superposition of the five
 317 molecules of SAT2/G-g3C^{pro}(1-208) in the asymmetric unit of the crystal, shown in ribbon
 318 representation. (d) Comparative superposition of SAT2/G-g3C^{pro}(1-208) (teal) with A10₆₁

319 3C^{pro} in the absence (purple; PDB 2J92)) and presence (orange; PDB 2WV4)) of a peptide
320 substrate (shown in stick representation).
321

322 **TABLE 1:** DNA primers for cloning and mutagenesis

Forward	SAT2/GHA/8/91 GATGATCTCGAGGAAGTGGCGCTCCGCCGACCGAC
Reverse	CATGCCAAGCTTATGGGTCAATGTGTGCTTTGAGTTGGAGCAGGCTCGACCGTG
C142A-for	GGACCAAGGTTGGATAC <u>CGCT</u> GGAGGAGCCGTCATGAC
C142A-rev	GTCATGACGGCTCCTCCAGCGTATCCAACCTTGGTCC
C163A-for	CATACAAAGATGTTGTCGTC <u>CGCC</u> ATGGACGGTGAACACCATGC
C163Arev	GCATGGTGTACCGTCCATGGCGACGACAACATCTTTGTATG
Forward	SAT1/NIG/5/81 GATGATCTCGAGGAAGTGGAGCGCCACCCACCGAC
Reverse	CATGCCAAGCTTAAGGGTCGATGTGTGCCTTCATC
C142A-for	GCCACCAAAGCTGGTTAC <u>CGCT</u> GGAGGAGCCGTTCTTG
C142A-rev	CAAGAACGGCTCCTCCAGCGTAACCAGCTTTGGTGGC
C163A-for	CCTACAAAGACATCGTAGTGGCTATGGATGGTGACACCATGC
C163Arev	GCATGGTGTACCATCCATAGCCACTACGATGTCTTTGTAGG
Forward	SAT1/UGA1/97 GATGATCTCGAGGAAGCGGTGCGCCACCGACCGAC
Reverse	CATGCCAAGCTTATGGGTGATGTGGGCTTTCATC
C142A-for	GGACCAAGGTAGGTTAC <u>CGCT</u> GGGGCGGCCGTAAGTAC
C142A-rev	GTCAGTACGGCCCGCCAGCGTAACCTACCTTGGTCC
C163A-for	GTACAACGACATCGTCGTC <u>CGCC</u> ATGGACGGCGACACCATG
C163Arev	CATGGTGTGCGCGTCCATGGCGACGACGATGTCGTTGTAC
Forward	SAT2/ZIM/7/83 GATGATCTCGAGGAAGCGGAGCCCCACCGACCGAC
Reverse	CATGCCAAGCTTAAGGGTCGATGTGGGCTTTCATC
C142A-for	GGGACCAAAGTGGATAC <u>CGCT</u> GGAGCCGCTGTTCTCG
C142A-rev	CGAGAACAGCGGCTCCAGCGTATCCAACCTTGGTCCC
C163A-for	CCTACAAAGACCTAGTCGTT <u>GCT</u> ATGGACGGTGAACACCATGC
C163Arev	GCATGGTGTACCGTCCATAGCAACGACTAGGTCTTTGTAGG

323

324

325 **TABLE 2:** Crystallographic data collection and model refinement statistics for SAT2 3C^{pro}.

DATA COLLECTION	
Space-group	P3 ₂
a, b, c (Å)	54.0, 54.0, 318.5
α, β, γ (°)	α = β = 90; γ = 120
Resolution range (Å)	53.1-3.2 (3.37-3.2)
No. of independent reflections	17053
Multiplicity¹	2.7 (2.7)
Completeness (%)	99.3 (99.5)
I/σ_I	5.7 (1.7)
R_{merge} (%)²	11.6 (42.4)
MODEL REFINEMENT	
No. of Non-hydrogen atoms	7535
R_{work} (%)³	22.2
R_{free} (%)⁴	27.2
Average B-factor (Å²)	119
RMS deviations - Bonds (Å)⁵	0.006
RMS deviations - Angles (°)	1.1
Ramachandran plot (favoured/allowed) %	89.8/10.2
PDB Accession Code	4X2Y

326

327 ¹Values for highest resolution shell given in parentheses328 ²R_{merge} = 100 × Σ_{hkl} |I_j(hkl) - <I_j(hkl)>| / Σ_{hkl} Σ_j I(hkl), where I_j(hkl) and <I_j(hkl)> are the

329 intensity of measurement j and the mean intensity for the reflection with indices hkl,

330 respectively.

331 ³R_{work} = 100 × Σ_{hkl} ||F_{obs}| - |F_{calc}|| / Σ_{hkl} |F_{obs}|.

332 $^4R_{\text{free}}$ is the R_{model} calculated using a randomly selected 5% sample of reflection data that
333 were omitted from the refinement.

334 ^5RMS , root-mean-square; deviations are from the ideal geometry defined by the Engh and
335 Huber parameters (Engh & Huber, 1991).

336